THE JOURNAL OF PHYSICAL CHEMISTRY A

Article

pubs.acs.org/JPCA

Femtosecond Photodetachment of Silver Anions

Benkang Liu,[†] Tao Long,[‡] Yanqiu Wang,[†] and Li Wang*[,†]

[†]State Key Laboratory of Molecular Reaction Dynamics, Dalian Institute of Chemical Physics, Chinese Academy of Science, Dalian 116023, People's Republic of China

[‡]Beijing SHRIMP Center, Beijing 100037, China

ABSTRACT: The two- and three-photon detachment of negative silver ions in a femtosecond infrared laser field is studied using photoelectron velocity map imaging methods. Photoelectron angular distributions (PADs) are obtained for these detachment channels; these PADs change dramatically when the laser wavelength and intensity are changed. Theoretical predictions, which are based on the adiabatic Keldysh−Faisal−Reiss saddle point method, are in good agreement with our experiment. The dependence of the PAD on the laser wavelengths and intensities is due to the interference between the different partial wave functions. The relative contributions of the different partial waves to the detachment amplitude are altered by changing the laser parameters and, as a result, the shape of the PAD. Close to the detachment threshold, the two-photon detachment process also follows the Wigner threshold law. Near the detachment threshold, the large differences between the calculated results and our experimental results indicate that the ponderomotive energy shifts caused by the femtosecond laser fields must be taken into account in the theoretical model. The three-photon detachment of Ag^- is also observed and compared with theoretical calculations.

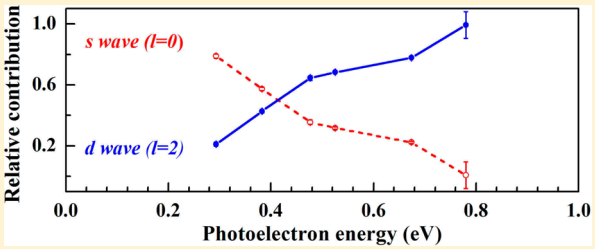

1. INTRODUCTION

In neutral atoms and positively charged ions, electrons are bound in a long-range Coulomb potential, which is proportional to r^{-1} (r is the separation between the electron and the nucleus). However, the excess electrons in negative ions are bound in a short-range potential on the order of r^{-4}, with the H^- ion being the only exception.[1] This short-range potential gives rise to a number of exotic properties of negative ions that are unlike those of neutral atoms or positive ions. Furthermore, the filling order of an excess electron into the electronic subshell may be different from that for the same neutral atom.[2,3] In an anionic atomic system, electron correlation effects often account for most of the features of the anions, such as the binding energy and the energetic positions and lifetimes of the excited states.

The photodetachment of "extra" electrons from anions has been proven to be the most accurate technique for investigating the structural properties of anions by studying the kinetic energy and angular distribution of the photodetached electrons. The photodetachment process is a bound-free transition, which provides a unique opportunity to examine electrons leaving a neutral atomic core in the presence of short-ranged potentials. Thus, subtle interactions, such as electron correlation and relativistic effects, which may be veiled by the long-range Coulomb potential present in the photoionization of neutral species or positive ions, can be investigated in photodetachment studies.[1] Interesting phenomena, such as the above-threshold detachment,[4−7] two-electron photodetachment,[8] and electron rescattering[9,10] of the negative ions, were investigated and characterized experimentally.

Various photodetachment techniques have been developed to address different aspects of anion research. For example, the K-shell photodetachment of Li^- using synchrotron light revealed a dramatically different structure than those of atoms and positive ions.[11] The experimental observations of the excess photon detachment of negative ions was reported in 1991 for Cl^- and Au^- systems and was similar to the above-threshold ionization or excess photon ionization in neutral or cation systems.[4,5] The electron energy spectrum and a dependence of the detachment rate on the laser intensity were obtained experimentally. The electron kinetic energy spectrum of F^- extended far beyond the classical cutoff value and appeared as a pronounced plateau localized within a small angle along the laser polarization axis.[10] The validity of the Wigner threshold law has been repeatedly demonstrated in negative-ion photodetachment spectroscopy.[1−3,12,13] Previous reports determined that the detachment process near the negative threshold followed the Wigner threshold law.[12,13] In the vicinity of the detachment threshold, the photodetachment cross section has the form $\sigma \propto E^{2l+1}$, where l is the angular momentum of the outgoing electron and E is its excess energy. Short-range final-state interactions can affect the range of the validity of the Wigner law but do not alter its form. In the case of Cl^-, the detached electron energies were less than 0.125 eV.[12] The photodetachment of anions in the vicinity of the detachment threshold has drawn attention because, in this energy range, the electron-correlation effects and interferences become more prominent.

Photoelectron angular distributions (PADs) have proven to be very important in elucidating the mechanisms that govern the

Received: May 22, 2013
Revised: October 9, 2013
Published: October 10, 2013

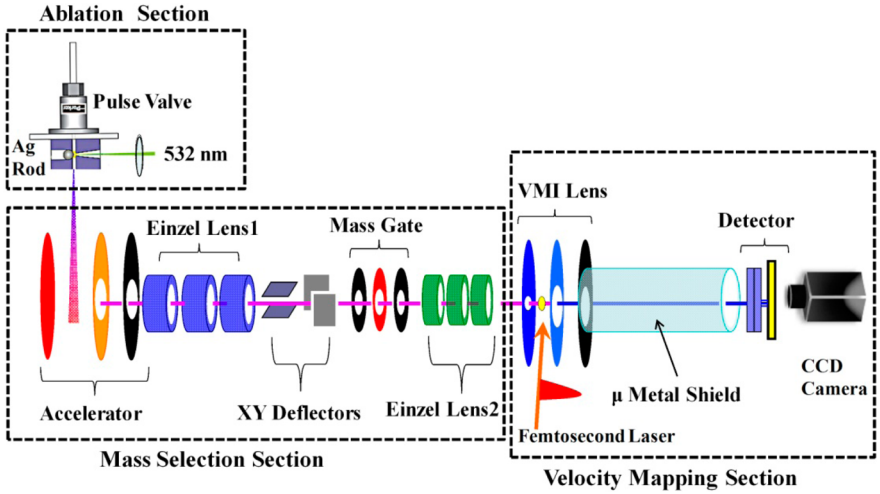

Figure 1. Schematic drawing of the experimental setup.

photodetachment processes. Specifically, in multiphoton detachment by a linearly polarized laser field, the quantum interference effects of the electrons emitted in such a process show a characteristic distribution in the angle-resolved energy spectrum.[6−8] Various theoretical models had been proposed to interpret the above-mentioned experimental results. Semianalytical approaches, such as the adiabatic saddle point model of Gribakin and Kuchiev[14,15] based on the original Keldysh approximation,[16] have been successfully applied in quantitatively describing the interaction of negative atomic ions with femtosecond[9,17] and few-cycle ultrafast infrared laser fields.[18,19]

The dependence of PADs on the laser intensity was predicted theoretically by the time-dependent Schrödinger equation using the Sturmian−Floquet approach.[20] Photoelectron velocity imaging may provide the kinetic energy and angular distribution of detached electrons simultaneously.[21] A one-photon detachment study of Cu^- showed no evidence of electron correlation effects at different laser wavelengths.[5] A single-photon detachment process resulted in an electron continuum with a single orbital angular momentum, $l = 1$ (for a p wave). The asymmetry parameter reduced to an energy-independent value of $\beta = 2$. The lowest photoelectron energy used in these experiments was either 0.682[22] or 1.08 eV.[23] However, this conclusion for one-photon detachment is different than that for the multiphoton detachment process of an anion. Among the various anions, the hydrogen anion H^- has been thoroughly studied both experimentally and theoretically in this energy range. For example, in the two-photon detachment experiment of H^- using a 2.15 μm infrared 250 fs laser field, the PAD was found to change dramatically with laser intensity. At an intensity of 6.5 $\times$ 10^{11} W/cm^2, the PAD had a bell-like appearance with the maximum pointing perpendicular to the laser polarization. The semiclassical KFR theory was used to explain this behavior.[6] A detached electron could tunnel into the continuum at different times within a period of the field oscillation, resulting in a continuum of wave functions with different phases at which electrons were emitted. The superposition of these wave functions with different phases led to a specific PAD dependence on the laser intensity. Nonperturbative Floquet theory predicted that, while the laser field intensity was fixed, similar effects would be observed under different laser frequencies.[24]

In this work, we report the results of photoelectron imaging experiments of Ag anions using two-photon absorption with a femtosecond infrared laser in the vicinity of the detachment threshold from the $4d^{10}5s^2\ ^1S_0$ state to the $4d^{10}5s^1\ ^2S_{1/2}$ state. The binding energy of Ag^- is 1.3044 eV.[25,26] Although the dependence of the PAD on the frequency and intensity of a linearly polarized laser is predicted theoretically for H^-,[15,16,18,19,24,27−29] direct experimental evidence remains quite scarce,[7,22] especially for negative metal ions. Furthermore, the validity of the above-mentioned theoretical approaches to negative heavy metal ions remains unknown. Additionally, the dependence of the PAD from negative metal ions on the laser intensity and wavelength has seldom been addressed.[30,31]

To the best of our knowledge, this is the first femtosecond two-photon photodetachment experimental study of this anion species. Our motivations are to explore the influence of the wavelength and intensity of the femtosecond laser pulse on the multiphoton detachment of negative atomic ions and to verify the validity of the Keldysh-like theory and the Wigner threshold law in this energy range. We selected the negative silver ion as a candidate due to the following considerations. First, the photodetachment of Ag^- originates from the $4d^{10}5s^2$ configuration. The detachment 5s electron is close to the 4d inner shell, which will be helpful in exploring whether these inner subshells significantly affect the detachment process and break the Wigner threshold rule. Second, previous reports have indicated that semianalytical approaches, such as the adiabatic saddle point model of Gribakin and Kuchiev[15] based on the Keldysh theory,[16] could be used to qualitatively describe the detachment of some negative ions, such as H^-,[1,2] F^-,[9,14,17] and K^-.[32] Our experiments will be helpful in verifying the applicability of these approximations to a metal anions, in which the distance between the detachment electron and the atomic core is large and the detachment electron is close to the inner-shell electrons. The mass of Ag^- is large enough to minimize the influence of the translational velocity of the ion on the angular distribution of the photodetachment electrons, which is advantageous to obtaining high-resolution PADs. For comparison, we numerically calculated the PADs as a function of both energy and emission angle using the adiabatic saddle point model of Gribakin and Kuchiev.[15]

2. EXPERIMENTAL SECTION

The negative silver ions are formed from a laser vaporization metal cluster source, in which the second harmonic output (532

nm) of a neodymium-doped yttrium aluminum garnet laser (YAG laser, Quantel Brilliant) with a pulse duration of 5 ns operating at 20 Hz is focused on a rotating and translating silver rod to form a plasma. The metal plasma is then cooled by helium carrier gas (99.9%) that is introduced into the target region through a pulsed valve at a stagnation pressure of 0.4 MPa and then expanded into a three-electrode accelerator region, as illustrated in Figure 1.

In the accelerator region, the negative ions are extracted perpendicularly by a −1.4 kV pulse electric field applied to the acceleration electrodes, collimated, and aligned by $X-Y$ deflectors and the first Einzel lens into a three-electrode mass gate. Mass selection is achieved by applying a time-delayed, pulsed electric field to the middle electrode and then refocusing into the center of a velocity map ion imaging lens (VMI lens) by the second Einzel lens. The mass-selected negative ions are then photodetached by a time-delayed femtosecond laser pulse.

The femtosecond photoelectron imaging setup has been described elsewhere,[33] and only a brief sketch is provided here. Our solid-state femtosecond laser system consists of a seed oscillator, an amplifier with a stretcher, and a compressor. The fundamental outputs (centered at 810 nm with a 22 nm fwhm bandwidth) at a 20 Hz repetition rate with 10 mJ/pulse are used to pump a commercial optical parametric amplifier (Quantronix/Light Conversion, TOPAS) to generate tunable infrared linearly polarized light between 1000 and 1800 nm with a 120 fs duration (fwhm). The laser beam is focused with a 50 cm focal length lens, and its polarization direction is parallel to the detector plane. The focus size is measured by the pinhole method. The peak intensity in the interaction region can be changed from 10^{10} to 10^{12} W/cm^2.

The detached photoelectrons are extracted from the focus of a carefully designed ion lens, the voltages of which are set so as to achieve velocity map ion imaging conditions, into a 40 cm field-free, μ-metal shielded flight tube.[33] Photoelectrons are amplified by a two-stage microchannel plate (MCP) and light up a small spot on a fast phosphor screen. The light image from this screen is captured by a thermoelectrically cooled charge coupled device video camera (LAVISION Inc. Imager QE). These experimental images (raw images) are two-dimensional projections of the nascent three-dimensional velocity distribution of photoelectrons. The three-dimensional distributions (reconstruction image) of photoelectrons (kinetic energy distributions and the angular distributions) may be recovered from these raw images by the use of the inverse Abel transform. This reconstruction is done by the pBASEX program.[30,31]

3. RESULTS AND DISCUSSION

The photoelectron image (raw image) obtained from the single-photon detachment of Ag^- by the 810 nm femtosecond laser is shown in Figure 2a. Figure 2b illustrates the reconstructed image from Figure 2a by using the BASEX method.[30,31] Figure 2c shows the photoelectron spectrum of Ag^- in 810 nm one-photon detachment. The single peak in the photoelectron spectrum of Ag^- is assigned to the removal of an electron from the fully occupied 5s orbital of the anion to the ground state of the neutral atom, which corresponds to the Ag $^2S_{1/2}$ ($4d^{10}5s^1$) ← Ag^- $^1S_0$ ($4d^{10}5s^2$) transition. This peak is centered at an electron binding energy of 1.29 eV. Because the bandwidth of our femtosecond laser is approximately 22 nm at the fundamental output, the photon energy ranges from 1.51 to 1.55 eV. Considering this energy width, the binding energy of 1.29 eV obtained in our single-photon detachment experiment is quite close to the value

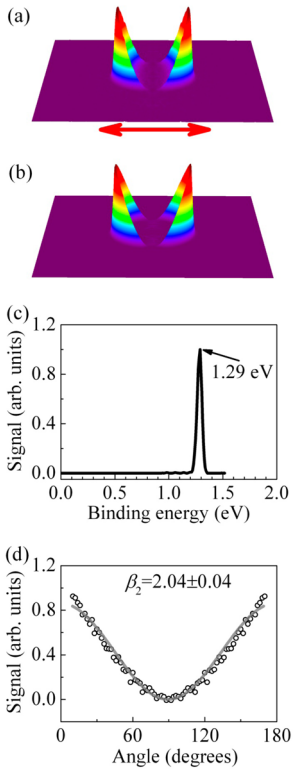

Figure 2. One-photon detachment result of Ag^- at 810 nm. (a) Raw photoelectron image, (b) reconstruction image, (c) photoelectron kinetic energy distribution obtained from (b), and (d) PAD obtained from (b) with the fitting result; empty circles: the experimental data; gray solid line: the fitting curve. The double-arrow line in (a) represents the direction of the laser polarization.

of 1.304 eV obtained using a narrow-bandwidth nanosecond laser.[23,26] Single-photon detachment can be described by a pure p wave function. The anisotropy parameter of the photoelectron image in Figure 2d, β_2, is approximately 2.04 ± 0.04, which is the same as that in Sobhy's experiment, 2.0 ± 0.06.[23,26]

In the case of the two-photon detachment process, the PADs show dramatic changes as the laser wavelength varies from 1191 (a) to 1555 (f) nm with a fixed laser intensity of 5.0×10^{10} W/cm^2, as shown in Figure 3. The excess energies of the detached electrons range from 0.29 (f) to 0.78 (a) eV. The PADs exhibit a structure that consists of a central jet and two main lobes. The lobes are located on either side of the central jet, and this structure closely resembles those found in the experiments on the multiphoton detachment of H^- and X^- (X = F, Br).[6−8] This similarity can be attributed to the short-range interaction between the weakly bound electron and the core of these negative ions, which exhibit similar behavior under the influence of external electromagnetic fields.

To understand the dependence of the PAD on the laser wavelength, we apply the saddle point method proposed by Gribakin and Kuchiev[15] that is based on the Keldysh theory.[16] According to this method, a simple analytical solution to the problem of multiphoton detachment by a monochromatic linearly polarized laser field $\mathbf{F}(t)=\mathbf{F}\cos\omega t$ can be obtained. The differential n-photon detachment rate of the negative ion, w_n, for the electron in the initial state l,m can be represented by the following

dx.doi.org/10.1021/jp405018r | J. Phys. Chem. A 2013, 117, 11210−11216

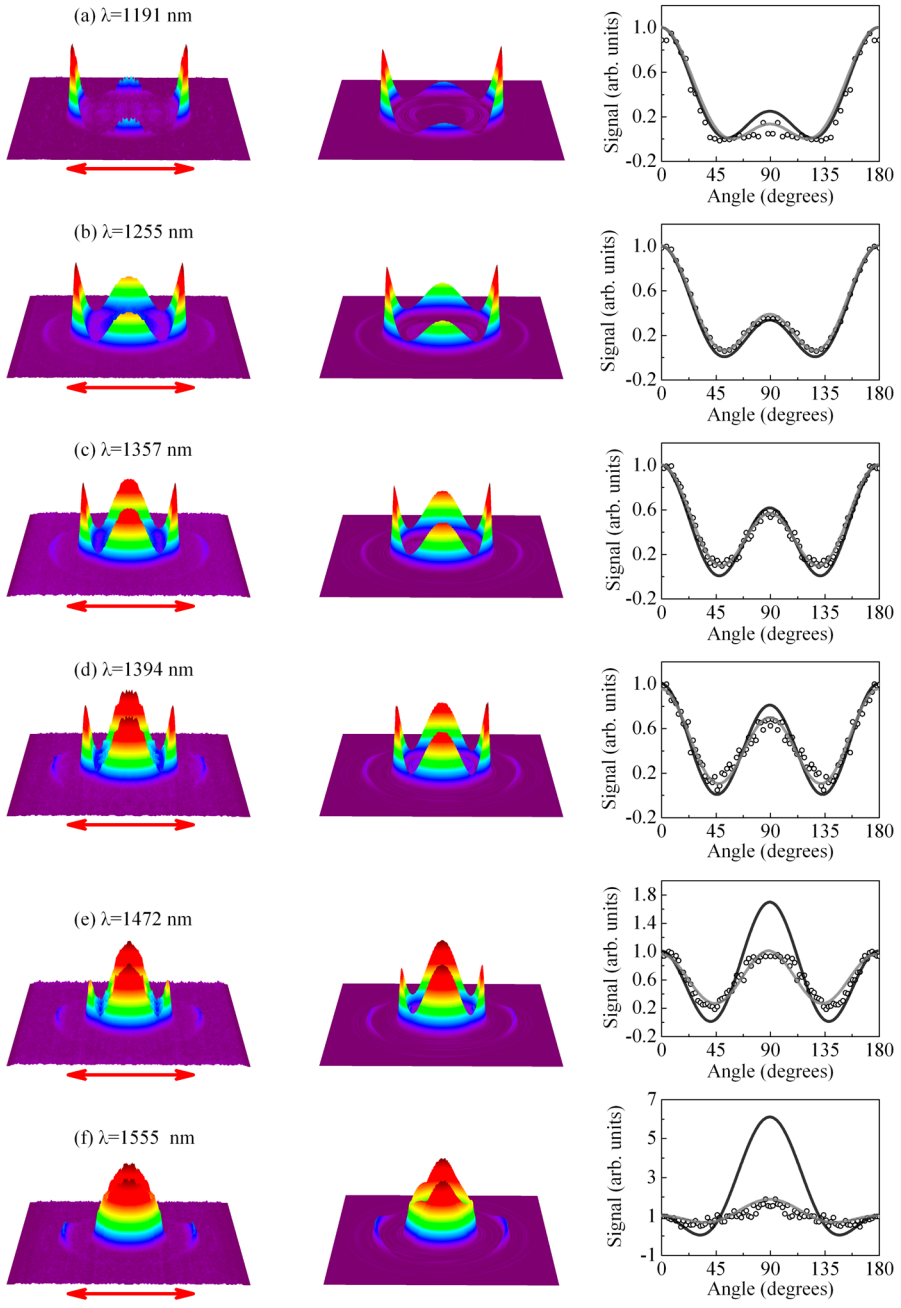

Figure 3. The two-photon detachment results of Ag^- in the laser field from 1191 to 1555 nm at a fixed intensity of 5.0×10^{10} W/cm^2. (Left column) Raw images; (middle column) reconstructed results; (right column) PADs. Empty circles in the right column: the experimental data; black lines: the calculated curves; gray lines: the fitting curves. Double-arrow lines in the left column represent the direction of the laser polarization.

$$\frac{dw_n}{d\Omega} = \frac{pA^2}{4\pi}(2l+1)\frac{(l-|m|)!}{(l+|m|)!} \times |P_l^{|m|}(\sqrt{1+p^2\sin^2\theta/\kappa^2})|^2 \times \left|\sum_{\mu=1,2}(\pm)^{l+m}\frac{(c_\mu+is_\mu)^n}{\sqrt{2\pi(-iS_\mu'')}}e - ic_\mu(\xi+zs_\mu)\right|^2 \quad (1)$$

$A = 1.3$ is the asymptotic parameter of the bound-state radial wave function of the Ag^- ground state, κ is determined from the energy of the bound state $E_0 \equiv -\kappa^2/2$, $p = [2(n\omega - (F^2/4\omega^2) + E_0)]^{1/2}$ is the photoelectron momentum, θ is the emission angle with respect to the polarization axis, $P_l^{|m|}$ is the associated Legendre function, $z = F^2/4\omega^3$, $\xi = Fp\cos\theta/\omega^2$, $s_\mu = (-\xi \pm i(8z(n-z) - \xi^2)^{1/2})/4z$, $c_\mu = \pm(1-s_\mu^2)^{1/2}$, $S_\mu'' = c_\mu(\xi + 4zs_\mu)$, and the $\pm$ signs in s_μ and c_μ correspond to the two saddle points $\mu = 1$ and 2. An explicit expression for the saddle points can be found in ref 15. This method has proven to be valid for describing the photodetachment process of anions.[6,7] The calculated results of Ag^- at different laser wavelengths are illustrated in the right column in Figure 3a–f. As illustrated in Figure 3, because relative intensities at different angles change heavily with the laser wavelengths, both the experimental results and calculation results are normalized at the angle of 5°, where the experimental results from 1191 to 1472 nm are the maxima intensities.

In this model, the dramatic changes in the PADs with the laser wavelength can be understood in terms of the quantum

dx.doi.org/10.1021/jp405018r | J. Phys. Chem. A 2013, 117, 11210−11216

interference of the electron trajectories.[6,15] According to this theory, an electron can be detached to the same final state at two instants of the laser field separated by $T/2$ when the field is close to the maximum, where T is the optical oscillation period of the laser. The relative phase of the corresponding wave functions of the emitted electrons varies with the phase of the field; thus, the interference of the wave functions produces oscillations in the photoelectron angular distribution. Here, using the Keldysh-like theory,[15] we have calculated the PADs of the emitted electrons after the two-photon detachment of Ag^-. As shown in Figure 3, this saddle point method[15] describes the PADs very well for shorter-wavelength detachment. For longer wavelengths, the differences between the theoretical predictions and our experimental results increase as the wavelength increases. One possible reason for this phenomenon is that, in close vicinity to the detachment threshold, the signal is very sensitive to the position of the quasienergy level, and the Keldysh-like theory does not take the quasienergy shift into account.

In the presence of linearly polarized monochromatic fields, the expression for the angular-resolved differential n-photon detachment rate can be expanded as a function of the angle, θ, between the detection and laser field directions on the basis of Legendre polynomials. Due to parity restrictions, only even Legendre polynomials are present in the expansion

$$\frac{d\Gamma_n}{d\Omega} = \frac{\Gamma_n}{4\pi}(1 + \sum_{l=1}^{\infty} \beta_{2l}^{(n)} P_{2l}(\cos\theta)) \quad (2)$$

where $\beta_{2l}^{(n)}$ are the anisotropy parameters and $P_{2l}(x)$ are the Legendre polynomials. In the case of weak and medium-strong external laser fields, lowest-order perturbation theory (LOPT) can be applied to simulate the two-photon detachment.[24] The detached electrons may have an angular momentum of 0 or 2, that is, s and d waves are mixed in the final state. For the two-photon detachment of Ag^-, according to LOPT, the emitted electrons may have an angular momentum of 0 and 2, which is a superposition of s and d waves in the final state. Even for intensities as high as 4×10^{11} and 6.5×10^{11} W/cm^2, the PADs can be well described by a superposition of s and d partial waves in two-photon detachment.[24] Because the intensity in this set of experiments is approximately 5.0×10^{10} W/cm^2, an explanation of the PADs can be provided within LOPT. Thus, the dependence of the detachment amplitude on the angle θ can be expressed as follows

$$\delta\sqrt{1/2}\,P_0(\cos\theta) + \sqrt{5/2}\,P_2(\cos\theta) \quad (3)$$

where the factors $(1/2)^{1/2}$ and $(5/2)^{1/2}$ are added as normalization coefficients for the Legendre polynomials. By fitting the experimental results, we can calculate the relative contributions of the s and d waves

$$P_s = \frac{|\delta|^2}{(1 + |\delta|^2)} \qquad P_d = \frac{1}{(1 + |\delta|^2)} \quad (4)$$

The relative contributions of the s and d waves at different laser wavelengths are illustrated in Figure 4. Near the detachment threshold (with excess energy less than 0.5 eV), P_s dominates the photodetachment amplitude. As the excess energy increases, the contribution of the d-wave component to the detachment signal becomes prominent. This phenomenon is in agreement with the Wigner threshold law.[13] According to this law, the two-photon detachment cross section scales as $E^{l+1/2}$, where E is the energy and l is the angular momentum of the emitted electron; thus, the

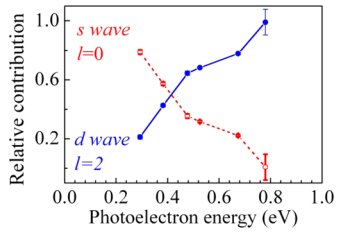

Figure 4. Partial-wave contributions to the two-photon detachment in the laser field from 1555 to 1191 nm at a fixed intensity of 5.0×10^{10} W/cm^2.

s wave dominates near the threshold. This tendency is indeed observed in our experiment, which confirms that the threshold effect is controlled by the Wigner threshold law.

Figure 5 shows three photoelectron images of the multiphoton detachment of Ag^- at the wavelength of 1357 nm with different intensities of 3.0×10^{10} (a), 6.0×10^{10} (b), and 1.6×10^{11} (c) W/cm^2. The PADs of the two-photon detachment channel are extracted from the images and shown in the right column. The solid lines are the calculation results described above. It is evident that the ratio of the height of the central jet to that of the main lobe increases with the laser intensity. Similar to the wavelength dependence, this PAD behavior can be attributed to the Wigner threshold law.[13] As explained by Telnov and Chu,[24] when the laser intensity increases with a fixed wavelength, the larger ponderomotive shift results in a drift of the two-photon detachment channel toward the detachment threshold, which changes the relative contributions of the s and d waves to the detachment amplitude and, as a result, the shape of the PADs.

Theoretical calculations and experimental PADs of the first-order above-threshold detachment (three-photon detachment channel) at wavelengths of 1375 (a) and 1555 (b) nm with a laser intensity of approximately 6.0×10^{10} W/cm^2 are illustrated in Figure 6. The PADs show a two-peak structure, which has been both experimentally observed and theoretically predicted in the H^- and X^- (X = F, Br) anion systems.[6−8,18,19] Using the method mentioned above, we calculated these three-photon detachment processes and compare them with the experimental results. On the basis of LOPT, the detached electron can be in either a p or f state in the case of three-photon detachment. The detachment amplitude at the angle θ can be simply expressed as

$$\delta\sqrt{3/2}\,P_1(\cos\theta) + \sqrt{7/2}\,P_3(\cos\theta) \quad (5)$$

where the factors $(3/2)^{1/2}$ and $(7/2)^{1/2}$ are added as normalization coefficients for the Legendre polynomials. By fitting the experimental results, the contributions of the p and f waves and the corresponding anisotropy parameters are obtained and tabulated in Table 1. As shown in Table 1, the relative weight of the p wave is much less than that of the f wave, while the excess energy of the detached electron is smaller. This result does not contradict the Wigner threshold law because the excess energy is much higher than the threshold.

4. SUMMARY

In summary, we report the multiphoton detachment results from the photoelectron imaging experiments of the Ag anion using a linearly polarized infrared femtosecond laser. While our single-photon detachment experiment of Ag^- gives the same conclusions as previous nanosecond experiments, the two-photon detachment experiments show very different characteristics. The photoelectron angular distributions in the two-photon

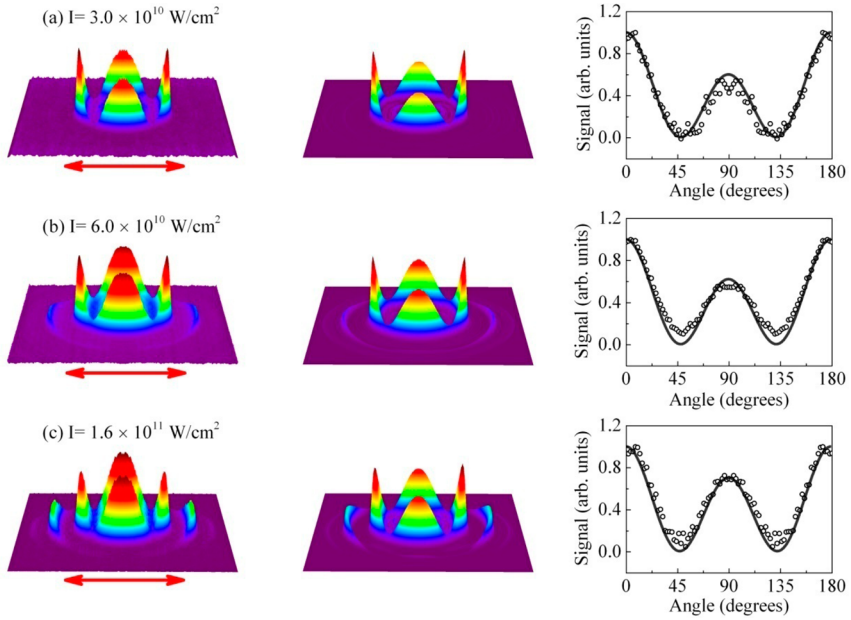

Figure 5. The two-photon detachment results of Ag^- from 3.0×10^{10} to 1.6×10^{11} W/cm^2 at 1357 nm. (Left column) Raw images; (middle column) reconstructed results; (right column) corresponding PADs. Empty circles in right column: the experimental data; black lines: the calculated curves; gray lines: the fitting curves. The double-arrow lines in the left column indicate the direction of the laser.

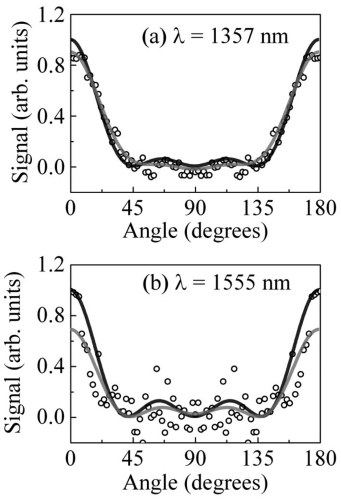

Figure 6. PADs of the three-photon detachment at wavelengths of 1357 and 1555 nm at a fixed intensity of 6.0×10^{10} W/cm^2; empty circles: the experimental data; black lines: the calculated curves; gray lines: the fitting curves.

Table 1. Anisotropy Parameters and Partial-Wave Contributions of the Three-Photon Detachment Channel

wavelength (nm)	β_2	β_4	β_6	P_p (%)	P_f (%)
1357	1.82 ± 0.06	1.47 ± 0.07	0.75 ± 0.06	75	25
1555	2.1 ± 0.5	2.8 ± 0.6	2.5 ± 0.6	18	82

detachment experiments exhibit structures containing main lobes along the laser polarization direction and central jet lobes perpendicular to the main lobes. The ratio of the jet lobe to the main lobe depends on the femtosecond laser wavelength and intensity. This PAD structure can be explained and well-reproduced theoretically. The relative weight of the s electrons increases when the two-photon detachment channel approaches the threshold. The wavelength dependence of the PADs of the first-order above-threshold detachment (three-photon detachment) is also shown and well-reproduced theoretically. To the best of our knowledge, this is the first femtosecond multiphoton detachment experiment of Ag^- close to the detachment threshold. Comparisons between our experimental results and theoretical predictions indicate that near the detachment threshold, the ponderomotive energy shift from the laser field must be taken into account in the new theoretical model.

AUTHOR INFORMATION

Corresponding Author

*E-mail: liwangye@dicp.ac.cn. Tel: +86-411-84379243. Fax: +86-411-84675584.

Notes

The authors declare no competing financial interest.

ACKNOWLEDGMENTS

This work was supported by the National Natural Science Foundation of China (Grants 21073188 and 21303199) and the National Major Scientific Instruments and Equipments Special Project of China (Grant 2011YQ05006903).

REFERENCES

(1) Andersen, T. Atomic Negative Ions: Structure, Dynamics and Collisions. *Phys. Rep.* **2004**, *394*, 157−313.

(2) Pegg, D. J.; Thompson, J. S.; Compton, R. N.; Alton, G. D. Evidence for a Stable Negative Ion of Calcium. *Phys. Rev. Lett.* **1987**, *59*, 2267−2270.

(3) Fischer, C. F.; Lagowski, J. B.; Vosko, S. H. Ground States of Ca^- and Sc^- from Two Theoretical Points of View. *Phys. Rev. Lett.* **1987**, *59*, 2263−2266.

(4) Davidson, M. D.; Muller, H. G.; van Linden van den Heuvell, H. B. Experimental Observation of Excess-Photon Detachment of Negative Ions. *Phys. Rev. Lett.* **1991**, *67*, 1712−1715.

(5) Stapelfeldt, H.; Balling, P.; Brink, C.; Haugen, H. K. Excess-Photon Detachment in the Negative Gold Ion. *Phys. Rev. Lett.* **1991**, *67*, 1731−1734.

(6) Reichle, R.; Helm, H.; Kiyan, I. Yu. Photodetachment of H^- in a Strong Infrared Laser Field. *Phys. Rev. Lett.* **2001**, *83*, 243001.
(7) Reichle, R.; Helm, H.; Kiyan, I. Yu. Detailed Comparison of Theory and Experiment of Strong-Field Photodetachment of the Negative Hydrogen Ion. *Phys. Rev. A* **2003**, *68*, 063404.
(8) Bergues, B.; Kiyan, I. Yu. Two-Electron Photodetachment of Negative Ions in a Strong Laser Field. *Phys. Rev. Lett.* **2008**, *100*, 143004.
(9) Pedregosa-Gutierrez, J.; Orr, P. A.; Greenwood, J. B.; Murphy, A.; Costello, J. T.; Zrost, K.; Ergler, T.; Moshammer, R.; Ullrich, J. Evidence for Rescattering in Intense, Femtosecond Laser Interactions with a Negative Ion. *Phys. Rev. Lett.* **2004**, *93*, 223001.
(10) Gazibegović-Busuladžić, A.; Milošević, D. B.; Becker, W.; Bergues, B.; Hultgren, H.; Kiyan, I. Yu. Electron Rescattering in Above-Threshold Photodetachment of Negative Ions. *Phys. Rev. Lett.* **2010**, *104*, 103004.
(11) Berrah, N.; Bozek, J. D.; Wills, A. A.; Turri, G.; Zhou, H. L.; Manson, S. T.; Akerman, G.; Rude, B.; Gibson, N. D.; Walter, C. W.; et al. *K*-Shell Photodetachment of Li^-: Experiment and Theory. *Phys. Rev. Lett.* **2001**, *87*, 253002.
(12) Trainham, R.; Fletcher, G. D.; Larson, D. J. One- and Two-Photon Detachment of the Negative Chlorine Ion. One- and Two-Photon Detachment of the Negative Chlorine Ion. *J. Phys. B: At. Mol. Phys.* **1987**, *20*, L777−L784.
(13) Wigner, E. P. On the Behavior of Cross Sections Near Thresholds. *Phys. Rev.* **1948**, *73*, 1002−1009.
(14) Kiyan, I. Yu.; Helm, H. Production of Energetic Electrons in the Process of Photodetachment of F^-. *Phys. Rev. Lett.* **2003**, *90*, 183001.
(15) Gribakin, G. F.; Kuchiev, M. Yu. Multiphoton Detachment of Electrons from Negative Ions. *Phys. Rev. A* **1997**, *55*, 3760−3771.
(16) Keldysh, L. V. Ionization in the Field of a Strong Electromagnetic Wave. *Zh. Eksp. Teor. Fiz.* **1964**, *47*, 1945−1957; *Sov. Phys. JETP* **1965**, *20*, 1307−1314.
(17) Bergues, B.; Ni, Y. F.; Helm, H.; Kiyan, I. Yu. Experimental Study of Photodetachment in a Strong Laser Field of Circular Polarization. *Phys. Rev. Lett.* **2005**, *95*, 263002.
(18) Shearer, S. F. C.; Smyth, M. C.; Gribakin, G. F. Electron Detachment from Negative Ions in a Short Laser Pulse. *Phys. Rev. A* **2011**, *84*, 033409.
(19) Shearer, S. F. C.; Addis, C. R. J. Strong-Field Photodetachment of H^- by Few-Cycle Laser Pulse. *Phys. Rev. A* **2012**, *85*, 063409.
(20) Krajewska, K.; Fabrikant, I. I.; Starace, A. F. Threshold Effects in Strong-Field Detachment of H^- and F^-: Plateau Enhancements and Angular Distribution Variations. *Phys. Rev. A* **2006**, *74*, 053407.
(21) Eppink, A. T. J. B.; Parker, D. H. Velocity Map Imaging of Ions and Electrons Using Electrostatic Lenses: Application in Photoelectron and Photofragment Ion Imaging of Molecular Oxygen. *Rev. Sci. Instrum.* **1997**, *68*, 3477−3484.
(22) Covington, A. M.; Duvvuri, S. S.; Emmons, E. D.; Kraus, R. G.; Williams, W. W.; Thompson, J. S.; Calabrese, D.; Carpenter, D. L.; Collier, R. D.; Kvale, T. J.; et al. Measurements of Partial Cross Sections and Photoelectron Angular Distributions for the Photodetachment of Fe^- and Cu^- at Visible Photon Wavelengths. *Phys. Rev. A* **2007**, *75*, 022711.
(23) Aravind, G.; Bhargava Ram, N.; Gupta, A. K.; Krishnakumar, E. Probing the Influence of Channel Coupling on the Photoelectron Angular Distribution for the Photodetachment from Cu^-. *Phys. Rev. A* **2009**, *79*, 043411.
(24) Telnov, D. A.; Chu, S. I. Angular Distributions from Two-Photon Detachment of H^- Near Ionization Threshold: Laser-Frequency and -Intensity Effects. *Phys. Rev. A* **2002**, *66*, 063409.
(25) Andersen, T.; Haugen, H. K.; Hotop, H. Binding Energies in Atomic Negative Ions: III. *J. Phys. Chem. Ref. Data* **1999**, *28*, 1511−1533.
(26) Sobhy, M. A.; Castleman, A. W., Jr. Photoelectron Imaging of Copper and Silver Mono- and Diamine Anions. *J. Chem. Phys.* **2007**, *126*, 154314.
(27) Borca, B.; Frolov, M. V.; Manakov, N. L.; Starace, A. F. Threshold Effects on Angular Distributions for Multiphoton Detachment by Intense Elliptically Polarized Light. *Phys. Rev. Lett.* **2001**, *87*, 133001.
(28) Frolov, M. V.; Manakov, N. L.; Pronin, E. A.; Starace, A. F. Model-Independent Quantum Approach for Intense Laser Detachment of a Weakly Bound Electron. *Phys. Rev. Lett.* **2003**, *91*, 053003.
(29) Bai, L. H.; Zhang, J. T.; Zhang, X. M.; Xu, Z. Z. Angular Distributions of Multiphoton Detachment of H^- in Various Infrared Laser Fields. *Phys. Rev. A* **2006**, *74*, 025402.
(30) Garcia, G. A.; Nahon, L.; Powis, I. Two-Dimensional Charged Particle Image Inversion Using a Polar Basis Function Expansion. *Rev. Sci. Instrum.* **2004**, *75*, 4989−4996.
(31) O'Keeffe, P.; Bolognesi, P.; Coreno, M.; Moise, A.; Richter, R.; Cautero, G.; Stebel, L.; Sergo, R.; Pravica, L.; Ovcharenko, Y.; et al. Photoelectron Velocity Map Imaging Spectrometer for Experiments Combining Synchrotron and Laser Radiations. *Rev. Sci. Instrum.* **2011**, *82*, 033109.
(32) Lindahl, A. O.; Rohlén, J.; Hultgren, H.; Kiyan, I. Yu.; Pegg, D. J.; Walter, C. W.; Hanstorp, D. Threshold Photodetachment in a Repulsive Potential. *Phys. Rev. Lett.* **2012**, *108*, 033004.
(33) Liu, B. K.; Wang, Y. Q.; Wang, L. Femtosecond Multiphoton Ionization of Pyrrole. *J. Phys. Chem. A* **2012**, *116*, 111−118.